Available online at www.sciencedirect.com
ScienceDirect
Polymer 49 (2008) 1943–1951
polymer
www.elsevier.com/locate/polymer

Melting behavior of poly(L-lactic acid): X-ray and DSC analyses of the melting process

Munehisa Yasuniwa*, Kazunari Sakamo, Yoshinori Ono, Wataru Kawahara

Department of Applied Physics, Faculty of Science, Fukuoka University, 8-19-1 Nanakuma, Jonan-ku, Fukuoka 814-0180, Japan

Received 6 December 2007; received in revised form 6 February 2008; accepted 18 February 2008
Available online 23 February 2008

Abstract

To clarify the melting behavior of poly(L-lactic acid) (PLLA), the wide-angle X-ray diffraction patterns of the isothermally crystallized PLLA samples (ICSs) were successively obtained during heating. We have already suggested the discrete change in the crystallization behavior of PLLA at a crystallization temperature (T_c) of 113 °C ($=T_b$) and formation of two crystal modifications for the ICSs obtained in the temperature range $T_c \leq T_b$ and $T_c \geq T_b$. It was elucidated from the change in the X-ray diffraction pattern that the phase transition from the low-temperature crystal modification (α'-form) to the high-temperature one (α-form) occurred in a range 155–165 °C for the ICSs($T_c \leq T_b$), and that the crystal structure for the ICSs($T_c \geq T_b$) did not change. Recrystallization during heating, which is the origin of the multiple melting behavior, was proved by the increase in the diffraction intensity before steep decrease due to the final melting. A temperature derivative curve of the X-ray diffraction intensity almost coincided with the DSC melting curve.

Keywords: Poly(L-lactic acid); X-ray; Melting

1. Introduction

Melting behavior of a semi-crystalline polymer is one of the most important characteristics of its physical properties, therefore much effort has been continuously paid to clarify it. As well known, the melting behavior largely depends on the preceding crystallization conditions of a sample and the heating conditions [1]. Since poly(L-lactic acid) (PLLA) is a typical semi-crystalline polymer, melting behavior of it has also been investigated in connection with the crystallization conditions [2–16]. The double melting behavior of a non-isothermally melt-crystallized PLLA sample has been reported and explained its origin by the melt-recrystallization model [7]. The double melting behavior of an isothermally melt-crystallized PLLA sample was studied by several authors [10,11,13,14,16]. Recently, Zhang and coworkers studied the heating process of PLLA by infrared spectroscopy [17]. They suggested the recrystallization and the change in the crystal structure during heating from the change in the characteristic crystalline and amorphous bands in the FTIR spectra.

Yasuniwa and coworkers carried out the isothermal crystallization of PLLA at various crystallization temperatures (T_cs) and elucidated that the crystallization behavior discretely changes at the crystallization temperature T_b ($=113$ °C) [18]. They also found that the crystal structure of the isothermally crystallized sample (ICS) discretely changes at T_b: The crystal structure of an ICS obtained at $T_c \leq T_b$ was obviously different from that of the ICS obtained at $T_b \leq T_c$. Based on these new facts on the crystallization behavior, we planned to clarify the melting behavior of PLLA, especially the effect of the discrete change in the preceding crystallization process on the melting behavior, in a series of articles.

In the first article of this series, the effects of crystallization temperature and crystallization time on the melting behavior of PLLA were studied with differential scanning calorimeter (DSC) using the ICS, and following points were elucidated [16]. (1) The T_c dependence of the melting temperature (T_m) discretely changed at T_b in accordance with the change in

* Corresponding author. Tel.: +81 92 871 6631; fax +81 92 865 6030.
E-mail address: yasuniwa@fukuoka-u.ac.jp (M. Yasuniwa).

0032-3861/$ - see front matter © 2008 Elsevier Ltd. All rights reserved.
doi:10.1016/j.polymer.2008.02.034

the crystal structure at T_b. (2) When T_c was lower than T_d ($T_c \leq T_d = 135$ °C), the double melting peaks appeared. In contrast, when T_c was higher than T_d, a single melting peak appeared. (3) T_c dependence of T_m discretely changed at T_b, and T_c dependence of dT_m/dT_c discretely changed at T_d. (4) The melting behavior, especially T_m and dT_m/dT_c, are different in three temperature regions of T_c divided by T_b and T_d: Regions I ($T_c \leq T_b$), II ($T_b \leq T_c \leq T_d$), and III ($T_d \leq T_c$).

Wide-angle X-ray diffraction (WAXD) measurement gives direct information on the crystal structure and crystallinity. The change in the crystal structure and the melt recrystallization in the heating process can be easily analyzed from the change in the WAXD pattern. According to this point of view, X-ray analysis on the melting process was performed to clarify the melting behavior of PLLA in this article. Especially, the analysis focused on the change in the crystal structure of the low-temperature crystal formed in Region I, which corresponds to the α′-form suggested by Zhang and coworkers [17,19], and the melting and recrystallization in the heating process in Regions I and II. Other background of this investigation was mentioned in the first article of this series [16], and relevant references on the melting behavior of PLLA were listed in it. Researches on the crystal structures and formation conditions of various crystal modifications of PLLA are in progress and are summarized elsewhere [17–21].

2. Experimental section

An additive free PLLA experimental resin (M_w: 10^5) in a pellet form was purchased from Polyscience Co. The pellets were heated and kept in a vacuum oven at 100 °C for 24 h for the removal of any residual moisture before they were measured.

A PLLA sample was sealed in a copper cylinder of 2.5 mm in inner diameter and 1 mm in height. Then the copper cylinder with the sample was capsulated in a DSC aluminum pan, and isothermal crystallization of the sample was carried out with DSC at a predetermined crystallization temperature (T_c). We could successfully obtain the samples with same thickness, 1 mm, by the use of the copper cylinder. The cylindrical sample, whose both ends were coated by epoxy resin to prevent moisture, was capsulated again in a DSC aluminum pan with a small hole at its center for the path of X-ray beam.

Wide-angle X-ray diffraction (WAXD) patterns were obtained during heating with a WAXD measurement system reported elsewhere [22]. Monochromatized Cu Kα radiation (= 1.542 Å) was used as an incident X-ray beam. The DSC pan, in which the cylindrical sample was capsulated, was set in a heating cell for the WAXD measurements. The diffracted X-ray was detected with a position-sensitive proportional counter (PSPC) system. The X-ray diffraction patterns in the heating process of ICSs were obtained at a heating rate of 1 K min^{-1}. To obtain an analyzable diffraction pattern in the heating process, the accumulation time of the PSPC for obtaining one pattern was set to 30 s, i.e. two patterns per minute and two patterns per Kelvin. The diffraction angles reported for α-aluminum oxide (α-Al_2O_3) were used as a standard: The angles of the diffraction patterns were corrected with three diffraction angles of α-Al_2O_3 for the Cu Kα radiation: 25.296°, 35.152°, and 37.801°, corresponding to the reflection lines of (012), (104), and (110), respectively [23]. Although correction of the diffraction angle was performed with this procedure, the absolute value of the diffraction angle has a slight experimental error ascribed to our homemade heating cell for the WAXD measurements [22].

Thermal analysis was carried out with a differential scanning calorimeter (Perkin–Elmer Pyris 1). The temperature of the DSC apparatus was calibrated with indium and tin. A PLLA sample of 5.0 ± 0.1 mg was sealed in an aluminum sample pan for DSC. Samples were always kept under a nitrogen atmosphere. Isothermal crystallization of the sample for the X-ray measurement and the DSC was carried out with DSC instrument by the same procedure described in the previous articles [16,18]. Temperature of a sample in the heating cell for the WAXD measurements was calibrated by its melting temperature obtained by DSC.

3. Results and discussion

3.1. Thermal analysis on the melting process

The melting behavior of PLLA largely changes by a heating rate [16]. Accordingly, at first, the melting process at a heating rate of 1 K min^{-1}, which was the same rate as for the X-ray measurement, was analyzed with DSC. Fig. 1 shows the

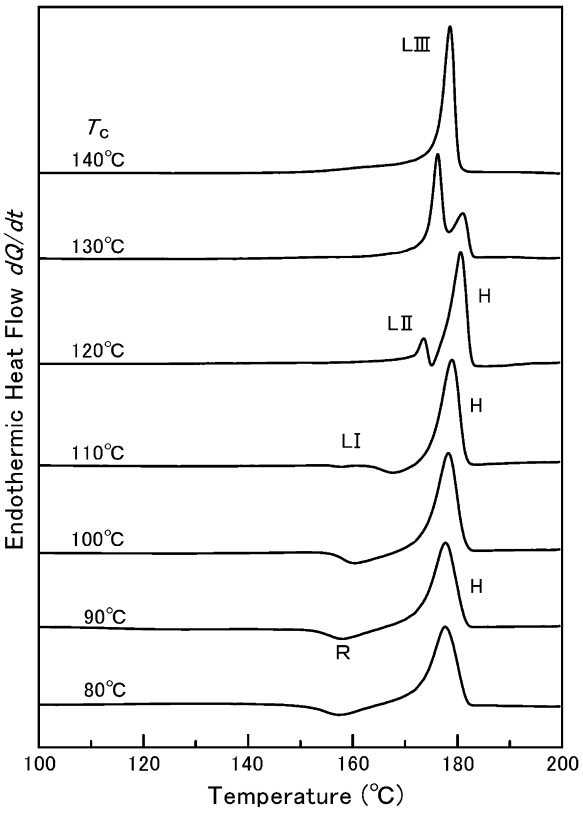

Fig. 1. DSC curves for the ICSs obtained at the indicated T_cs. The crystallization time for the ICSs of 80, 90, 100, 110, 120, 130, and 140 °C were 400, 120, 50, 30, 60, 190, and 540 min, respectively. Heating rate of the DSC scans was 1.0 K min^{-1}.

DSC curves of the ICSs(80–140 °C) during heating. T_c dependence of the DSC melting curves shown in the figure is almost coincides with that reported in the previous article of this series. T_b and T_d determined from the T_c dependence of T_m were approximately 113 and 135 °C, respectively. There are small differences in the values of T_b and T_d from those reported in the previous one. The small differences are deduced to be caused from the differences of the heating rate and the sample used as an original resin [16]. By the use of T_b and T_d, according to the interpretations reported in the previous article, T_c dependence of the melting behavior is also divided into three temperature regions: Regions I ($T_c \leq T_b$), II ($T_b \leq T_c \leq T_d$), and III ($T_d \leq T_c$). That is, the ICSs(80–110 °C), ICSs(120, 130 °C), and ICS(140 °C) are in Regions I, II, and III, respectively.

In the previous article, three types of peaks, L (LI, LII, LIII), R and H, appeared in the DSC melting curve. The peaks L, R, and H originate from the melting of original crystals, recrystallization, and the melting of recrystallized crystals, respectively. Outline of the mechanism for the appearance of these peaks has been explained elsewhere [7,16,22,24]. DSC peaks shown in Fig. 1 in this investigation were assigned according to the assignment of the previous article. A high-temperature endothermic peak (H) and a broad exothermic peak (R) appeared for the ICSs(Region I: 80–110 °C), whereas a low-temperature endothermic peak (LI) could not be observed except for the ICS(110 °C). In contrast, double endothermic peaks, LII and H, evidently appear for the ICS-(Region II: 120, 130 °C). The exothermic dip, which is located between LII and H, can be observed for the ICS(120, 130 °C). The T_c dependence of the increase and decrease in the double melting peaks in the DSC curves coincides with the interpretation of the melt-recrystallization model: as T_c increased, the peak L increased, whereas the peak H decreased. The DSC curve for the ICS(Region III: 140 °C) shows a single peak of LIII.

The crystal structures of the ICS($T_c \leq T_b$) and the ICS($T_b \leq T_c$) were assigned to trigonal (β-form) [25,26] and orthorhombic (α-form) [27–29], respectively. However, that of the ICS($T_c \leq T_b$) was not definitely determined because of a small number of the X-ray diffraction peaks. Recently, Zhang and coworkers showed that the crystal structure of the ICS($T_c \leq T_b$) is disordered phase of the α-form (orthorhombic), and they named it as "α′-form" [17,19]. Hereafter α′-form and α-form are used for the names of crystals in the ICS($T_c \leq T_b$) and the ICS($T_b \leq T_c$), respectively, according to their interpretation of the crystal structures of the ICS($T_c \leq T_b$) and notation. The names LTC and HTC used in the previous article correspond to α′-form and α-form, respectively [16].

DSC curve for the ICS(Region I: 80–110 °C) shows the melting process of the α′-form. According to the interpretation of the melt-recrystallization model, disappearance of LI in the DSC curve indicates that the melt recrystallization successively occurs in the heating process from a low temperature. The DSC melting curves for the ICS(Region II: 120, 130 °C) and ICS(Region III: 140 °C) represent the melting processes of the α-form with low and high thermal stabilities, respectively. The structural analysis on the melting process of the ICS will be shown in the subsequent sections.

3.2. X-ray diffraction patterns of ICSs at room temperature

Fig. 2 shows the X-ray diffraction patterns at room temperature of ICSs. Isothermal crystallization temperatures, T_cs, are indicated in the figure. As reported in Ref. [18], peak crystallization time largely changes with T_c, therefore different crystallization time is required to obtain the ICS for each T_c. According to the Ref. [18], the ICSs(80, 100, 120, and 140 °C) were obtained with the crystallization times of 400, 50, 60, and 540 min, respectively. The accumulation time of the PSPC of these patterns was 30 min, which was longer than that of the measurement (0.5 min) performed in the heating process, to obtain refined diffraction patterns of the present PLLA sample. Because there is scattering X-ray from the amorphous part on the diffraction intensity from the crystalline part, these diffraction patterns were obtained after the subtraction of an X-ray scattering pattern of the molten state of PLLA. The X-ray diffraction patterns shown in the subsequent sections were also processed ones by the subtraction procedure.

The X-ray diffraction patterns shown in this figure are almost the same as those shown in Fig. 8 in Ref. [18] in spite of the difference in the original resins. The diffraction angles

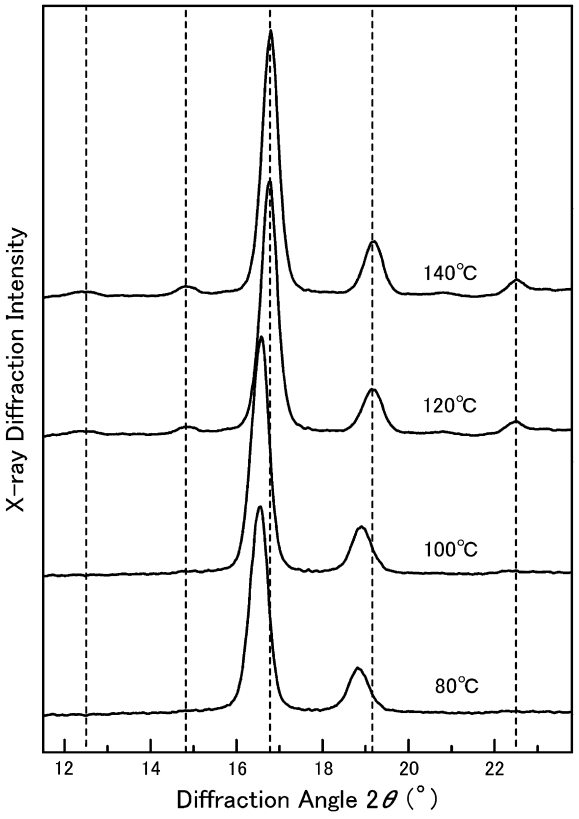

Fig. 2. X-ray diffraction patterns for the ICSs. Crystallization temperatures of the samples are shown. Dotted lines show diffraction angles of 12.5°, 14.8°, 16.8°, 19.2°, and 22.5° at which diffraction peaks for the ICS(140 °C) appear.

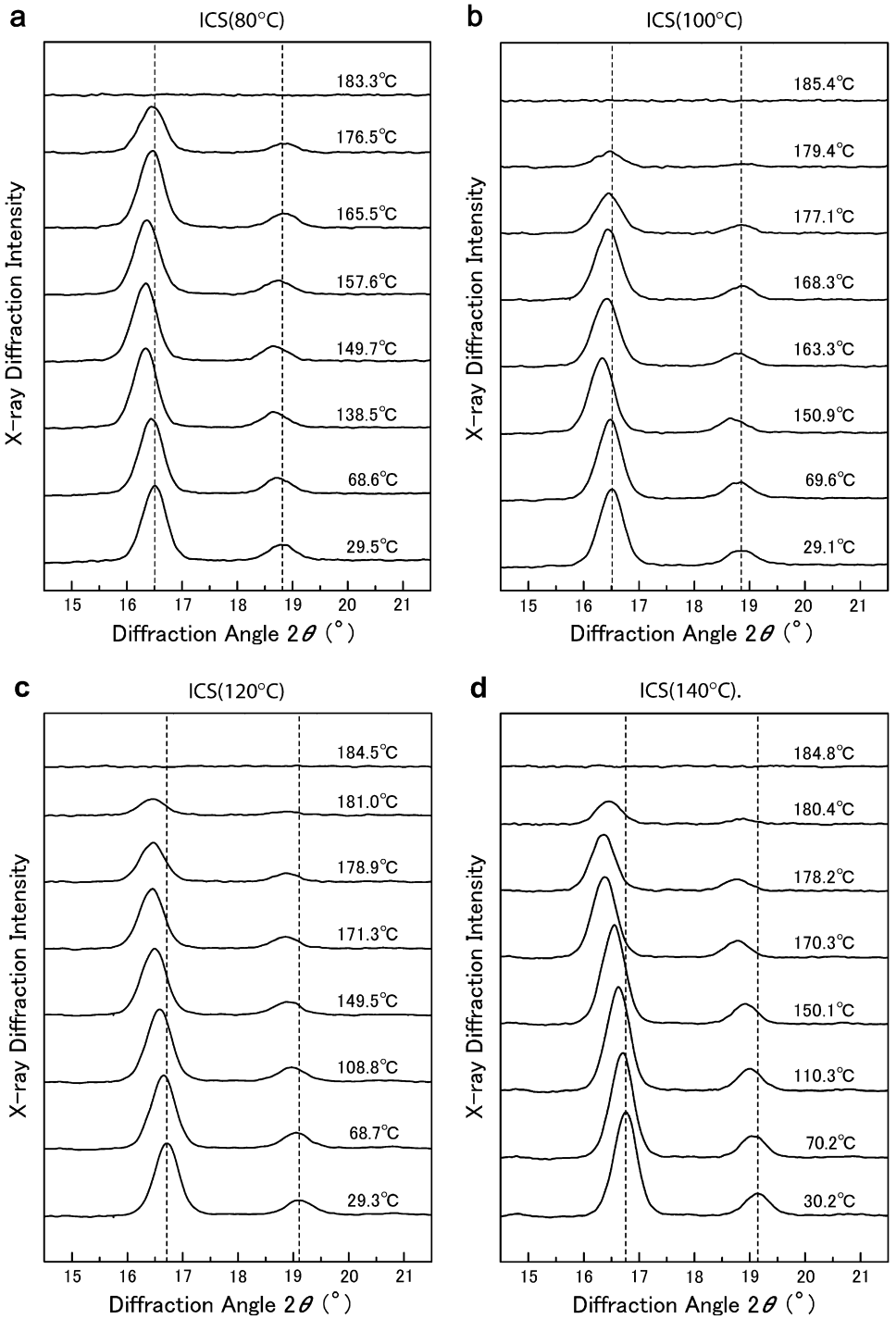

Fig. 3. X-ray diffraction patterns in the heating process: (a) ICS(80 °C), (b) ICS(100 °C), (c) ICS(120 °C), and (d) ICS(140 °C). Heating rate was 1.0 K min^{-1}.

of five peaks appeared in the diffraction patterns for ICSs($T_b \leq T_c$) are marked by dotted lines in the figure. There is clear difference between the diffraction patterns of ICSs($T_c \leq T_b$: 80, 100 °C) and ICSs($T_b \leq T_c$: 120, 140 °C): The most intense diffraction peak and the next one for ICSs($T_b \leq T_c$) shift to the lower diffraction angle in the diffraction patterns for ICSs($T_c \leq T_b$), and small diffraction peaks at 12.5°, 14.8° and 22.5° for ICSs($T_b \leq T_c$) disappear in the diffraction patterns for ICSs($T_c \leq T_b$). Accordingly, the difference in the crystal structure can be easily identified by the diffraction pattern with these characteristic diffraction peaks, especially the main peak and the next one.

3.3. X-ray diffraction patterns in the heating process

The X-ray diffraction patterns in the heating process for the ICSs(80, 100, 120, 140 °C) were obtained at a heating rate of 1 K min^{-1} and are shown in Fig. 3(a)–(d). The diffraction patterns were obtained at a rate of two patterns per Kelvin. The diffraction patterns more than 300 were obtained for

each ICS. The samples were covered by epoxy resin to prevent hydrolysis in the heating process so that the diffraction patterns shown in the figure result in somewhat diffuse one in comparison with those shown in Fig. 2. The diffraction angles of the main and sub peaks in the diffraction patterns of the starting temperature for each ICS are marked by dotted lines to distinguish the shift in the diffraction angle of the diffraction peaks.

The diffraction patterns shown in Fig. 3(a)–(d) almost coincide with corresponding diffraction patterns shown in Fig. 2, except for the slight shift in the diffraction angle due to the thermal expansion. Diffraction patterns shown in (a) and (b) were clearly different from those shown in (c) and (d). As described in the previous subsection, the α′-form and the α-form can be recognized by the two characteristic diffraction peaks and the five characteristic peaks, respectively.

The further analysis on the temperature dependence of the peak position and peak intensity of the X-ray diffraction peak and the correspondence between the X-ray analysis and DSC of the ICSs will be shown in subsequent subsections. Characteristics of the X-ray diffraction patterns in the three temperature regions, Regions I, II, and III, are as follows.

Region I. The diffraction peaks for the ICS(80 °C) shifted to a larger diffraction angle after the shift to a smaller angle in the heating process. The initial shift to the smaller angle in a low-temperature region corresponds to the thermal expansion, and the next shift to the larger angle in a high-temperature region corresponds to the transformation of crystal structure due to the transition from the α′-form to the α-form. To distinguish the appearance of the α-form in the heating process for the ICSs(80, 100 °C), the diffraction patterns enlarged in diffraction intensity are shown in Fig. 4. The dotted lines in Fig. 4 show the characteristic diffraction angle of the α-form at room temperature. Although there is a shift in each diffraction peak from the characteristic angle due to the thermal expansion, the five peaks corresponding to the formation of the α-form can be observed. That is, the transformation of crystal structure in the heating process from the α′-form to the α-form can be concluded from the appearance of the five characteristic peaks of the α-form. Temperature region where the diffraction peak shifts to the larger diffraction angle is between about 150 and 170 °C and agrees to that where the exothermic peak appears in the DSC curve shown in Fig. 1.

Region II. As shown in Fig. 3 (c), the diffraction pattern for the ICS(Region III: 120 °C), which corresponds to the orthorhombic, did not change over the whole temperature range, except for a change in the peak height due to the melting and a shift in the peak position due to the thermal expansion. This result gives a conclusion that the crystal structure does not change during the melting process in Region II. Although the double endothermic peaks in the DSC curve for the ICS(120 °C) have a possibility of the interpretation that the double melting is assigned to two different crystal structures, the X-ray result shown in (b) obviously denies this possibility.

Region III. The profile of the diffraction pattern shown in Fig. 3(d) for the ICS(Region III: 140 °C) is similar to that for the ICSs(120 °C), although there was small difference in the peak height between these samples. The diffraction pattern for the ICS(140 °C) also did not change over the whole temperature range, therefore the X-ray analysis also gives conclusion that the crystal structure of the α-form does not change during the melting process in Region III. Since the ICS(140 °C) shows a single DSC melting peak as shown in Fig. 1, the melting process suggested by X-ray analysis corresponds well with that suggested by DSC.

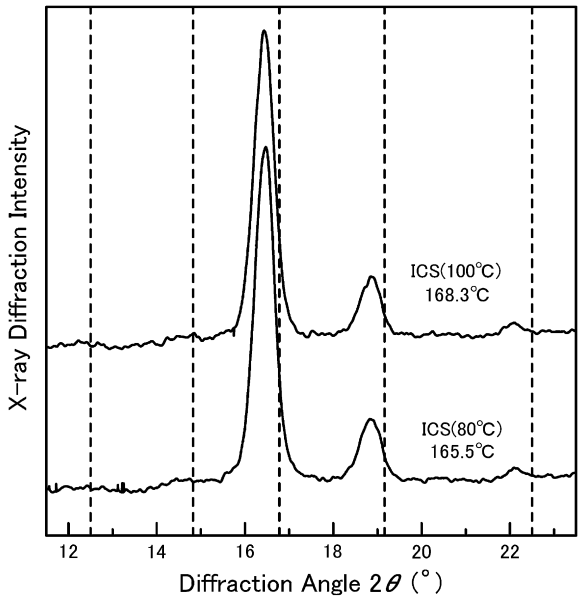

Fig. 4. Change in the X-ray diffraction pattern from the α′-form to the α-form for the ICSs($T_c \leq T_b$): (a) ICS(80 °C) and (b) ICS(100 °C).

3.4. Lattice spacing in the heating process

Lattice spacing was calculated from the diffraction angle of the X-ray diffraction peak by the use of Bragg's equation, $d = n\lambda/2 \sin\theta$; where d lattice spacing, n number of the order of reflection, λ wave length, θ diffraction angle. Although several diffraction peaks appear in the diffraction pattern, the lattice spacing in this study was calculated from the main peak at around 16.5° for ICSs(80, 100 °C) and 16.7° for ICSs(120, 140 °C). Because other diffraction peaks are small and broad compared with the main peak, the values of the diffraction angles could not be accurately determined. Therefore, the other peaks were not used for the calculation of the lattice spacing.

Fig. 5 shows temperature dependence of the lattice spacing d of ICSs(80, 100, 120, 140 °C). The values of d were calculated from the main peaks in the WAXD patterns of the ICSs. The lattice spacing for the ICSs increased almost linearly with temperature up to the melting temperature because of the thermal expansion of the crystal lattice, except for the temperature region around 155 °C for ICSs(80, 100 °C). According to the interpretation suggested by Zhang and coworkers [17,19], the α′-form is assigned to the disordered phase of the α-form (orthorhombic). Consequently, the main peak corresponds to

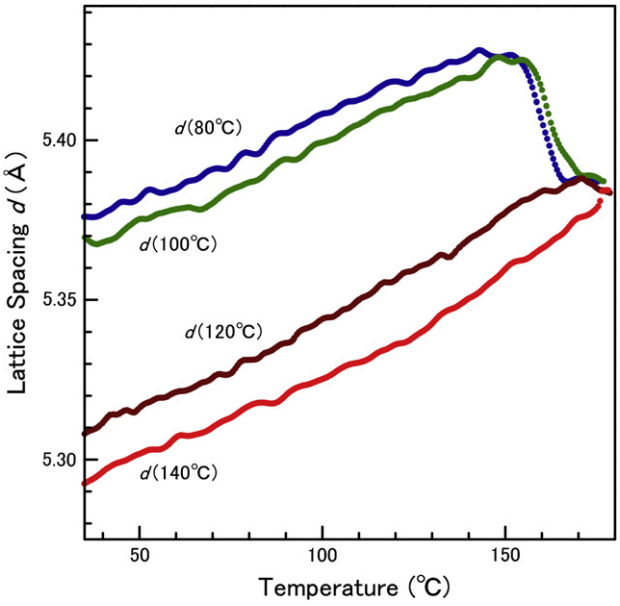

Fig. 5. Temperature dependence of the lattice spacing, $d(T_c)$, calculated from the angles of the main peak in the WAXD patterns of each ICS(T_c). T_cs are indicated. Heating rate was 1.0 K min^{-1}.

the combined peak of (110) and (200) reflections of the orthorhombic one. The next intense peak at around 18.8° for ICSs(80, 100 °C) and 19.1° for ICSs(120, 140 °C) corresponds to the (203) reflection.

It is easily recognized from the figure that the lattice spacing increases with increasing T_c. Especially, the lattice spacing for the ICSs(80, 100 °C) in a low-temperature region is evidently larger than that for the ICSs(120, 140 °C). That is, the lattice spacing of the α′-form (Region I) is larger than that of the α-form (Regions II and III) as suggested in Ref. [18].

As shown in the figure, the lattice spacing for the ICS(80, 100 °C) obviously decreased in the temperature region around 155 °C, and the values of the lattice spacing for the ICS(80, 100 °C) fall to those of the ICS(120, 140 °C) at about 165 °C. As mentioned in previous subsection, it was concluded from the appearance of the five diffraction peaks of α-form that the transformation of crystal structure from the α′-form to the α-form occurs in the same temperature region.

Since the lattice spacing for the ICSs increased almost linearly with temperature, temperature dependence of the lattice spacing can be fitted by the linear equation. The thermal expansion coefficients obtained from the fitting curve were 1.0×10^{-4} K^{-1} for ICSs(80, 100 °C) in the temperature range of 40–140 °C and 1.1×10^{-4} K^{-1} for ICSs(120, 140 °C) in the temperature range of 40–160 °C. This result suggests that the thermal expansion of ICS(Region I) is almost the same as that of ICS(Region II or III).

3.5. Melt recrystallization in the heating process

The melt-recrystallization model suggests that the small and/or imperfect crystals change successively to more stable crystals through melt-recrystallization process. That is, the melting and recrystallization are competitive in the heating process. The low-temperature and high-temperature endothermic peaks in the DSC melting curve appear when the rate of melting overwhelms that of the recrystallization, whereas the exothermic peak appears when the rate of recrystallization overwhelms that of the melting. Consequently, the recrystallization behavior, that is, the increase in crystallinity during the melting process, has an important role on the appearance of the double melting peaks.

Assuming that the width of a X-ray diffraction peak does not change much in the heating process of the sample, we use peak heights for the individual reflection lines instead of the diffraction intensity to estimate the quantity of crystallites in the sample, that is, crystallinity. Fig. 6 shows temperature dependence of the X-ray diffraction intensities of the main peak in the heating process of the ICSs at a heating rate of 1 K min^{-1}. T_cs of the ICSs are indicated in the figure. The diffraction intensities of the main peak in the X-ray diffraction pattern were obtained as a function of temperature. Hereafter, the X-ray diffraction intensity, endothermic heat flow, and lattice spacing are denoted by symbols I, dQ/dt, and d, respectively.

As shown in the figure, the diffraction intensities were almost constant during heating in the low-temperature region up to about 140 °C and decreased abruptly around 180 °C by the final melting. A positive peak of the diffraction intensity appeared in the temperature range between 160 and 180 °C whereas it is just before final melting for ICSs(T_c: 80, 100, 120 °C). The positive peak in Regions I(T_c: 80,

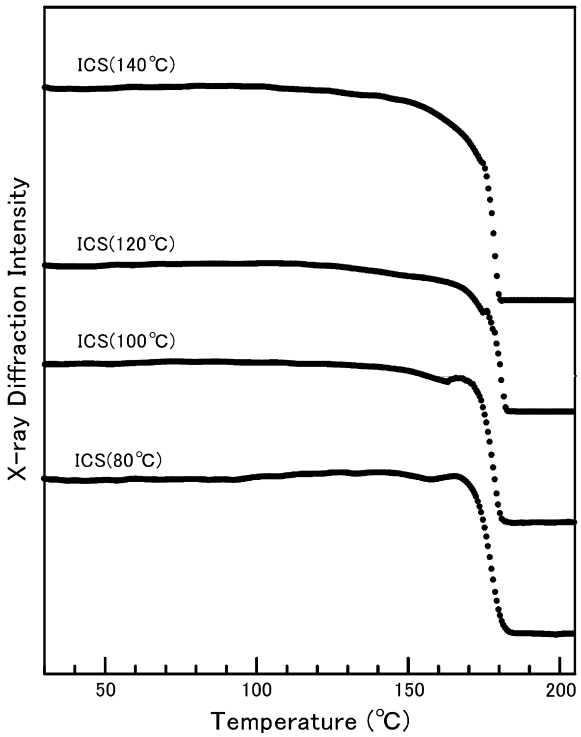

Fig. 6. Temperature dependence of the diffraction intensities in the heating process of the ICSs at a heating rate of 1.0 K min^{-1}. T_cs of the ICSs are indicated.

100 °C) is large and broad in comparison with that in Regions II(T_c: 120 °C). The peak temperature increases with increasing T_c. In contrast, ICS(Region III: 140 °C), the diffraction intensity monotonously decreases with temperature without the positive peak.

The appearance of the positive peak of the diffraction intensity before final melting indicates an increase in crystallinity during the melting process. Accordingly this peak is interpreted to be a solid proof of the recrystallization, and the exothermic peak in the DSC curve can be conclusively attributed to the recrystallization. In addition, the double melting behavior of PLLA is concluded to originate from the increase in crystallinity through recrystallization.

We have studied the double melting behavior of poly(butylene terephthalate) (PBT) and poly(butylene naphthalate) (PBN) with DSC and WAXD measurements [22,30,31]. The diffraction patterns of PBT and PBN in the heating process were obtained successively by the same X-ray measurement system used in this study. Recrystallization during the melting process of PBT and PBN was also confirmed by an increase in the X-ray diffraction intensity before final melting.

Recently, Zhang and coworkers studied the heating process of PLLA sample crystallized at 80 °C by infrared spectroscopy and showed increase in the peak heights of the crystalline band and decrease in amorphous band as a function of temperature during the heating process. They suggested the occurrence of the recrystallization or phase transition before final melting [17]. Similar results obtained by the infrared spectroscopy have been reported by other authors [20]. Their experimental results agree well with those obtained in the present investigation. On the other hand, FTIR spectra in their measurement were recorded at a rate of ~1 spectrum per Kelvin. In contrast, the diffraction patterns in the present investigation were obtained at a rate of two patterns per Kelvin. This difference means that the X-ray results give a detailed information on the heating process compared with those obtained before.

3.6. Correspondence between X-ray analysis and DSC

A change in the X-ray diffraction intensity $\Delta I(T)$ from T_0 to T is approximately proportional to the crystallinity change in the temperature range from T_0 to T. Endothermic heat flow dQ/dt of a sample can be obtained from a DSC curve so that endothermic heat change $\Delta Q(T)$ from T_0 to T with a constant heating rate R ($= dT/dt$) results in:

$$\Delta Q(T) = \int_{t_0}^{t} \left(\frac{dQ}{dt}\right) dt = \int_{T_0}^{T} \left(\frac{dQ}{dt}\right)\frac{dt}{dT}dT = \frac{1}{R}\int_{T_0}^{T} \left(\frac{dQ}{dt}\right) dT$$

where t_0 and t correspond to the times at the sample temperatures T_0 and T, respectively. The endothermic heat change $\Delta Q(T)$ takes positive value for the melting and is proportional to the decrease in crystallinity from T_0 to T. Therefore, $\Delta I(T)$ is approximately proportional to $-\Delta Q(T)$. In addition, temperature derivative curve of the diffraction intensity is also proportional to the heat flow curve, i.e. $dI/dT \propto -dQ/dt$. This relation means that the profile of a DSC curve can be obtained from the temperature derivative curve of the diffraction intensity. These relations among $\Delta I(T)$, $-\Delta Q(T)$, dI/dT, and $-dQ/dt$ are schematically illustrated in Fig. 7. As well known, the heat flow signal of DSC includes two components, latent heat and heat capacity. Therefore deviation from the above proportional relations mainly occurs when contribution due to the heat capacity largely increases.

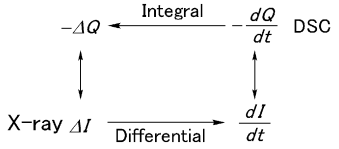

Fig. 7. Relations among ΔI, $-\Delta Q$, dI/dT, and $-dQ/dt$ obtained with DSC and X-ray measurement.

For the comparison of the data obtained with WAXD measurement and DSC, ΔI, $-\Delta Q$, dI/dT, and $-dQ/dt$ at a heating rate of 1 K min^{-1} are shown in the same figure (Fig. 8) on the same temperature scale. The figures for the ICSs(80, 100, 120, 140 °C) are shown in (a)–(d), respectively. Temperature dependence of the lattice spacing (d), which was shown in Fig. 5, is also shown in each figure. The endothermic heat change ($-\Delta Q$) and the endothermic heat flow ($-dQ/dt$) are expressed as a negative direction of the ordinate axis in this figure.

As shown in Fig. 8, the endothermic enthalpy change $-\Delta Q$ and the temperature derivative curve dI/dT approximately coincide with the diffraction intensity ΔI and the DSC curve $-dQ/dt$, respectively. The small difference between the temperature dependence of ΔI and $-\Delta Q$ (or dI/dT and $-dQ/dt$) may be caused from the contribution due to the heat capacity. It is noteworthy that DSC curve could be reproduced by a temperature derivative curve of the diffraction intensity.

3.7. Melting process

Characteristics of the melting process of Regions I, II, and III are summarized as follows.

Region I. As shown in Fig. 5, the lattice spacing d of the α'-form is larger than that of the α-form and increases with temperature by the thermal expansion. Thermal motion of PLLA molecular chain in the frustrated lattice of the α'-form increases with increasing temperature. As shown in Fig. 8(a), the lattice spacing decreases in the transition region around 160 °C for ICS(80 °C). The X-ray analysis indicates that the crystal to crystal phase transition from the α'-form to the α-form occurred in this temperature region, and that the crystallinity (ΔI, $-\Delta Q$) also increases through the reorganization of chain molecules. In case of the ICS(100 °C), the decrease in the lattice spacing (Fig. 5), the transition from the α'-form to the α-form (Fig. 8(b)), and the increase in the crystallinity occur around 165 °C. The increase in the crystallinity before final melting results in the appearance of exothermic and endothermic peaks in the DSC melting curve as shown in Fig. 8.

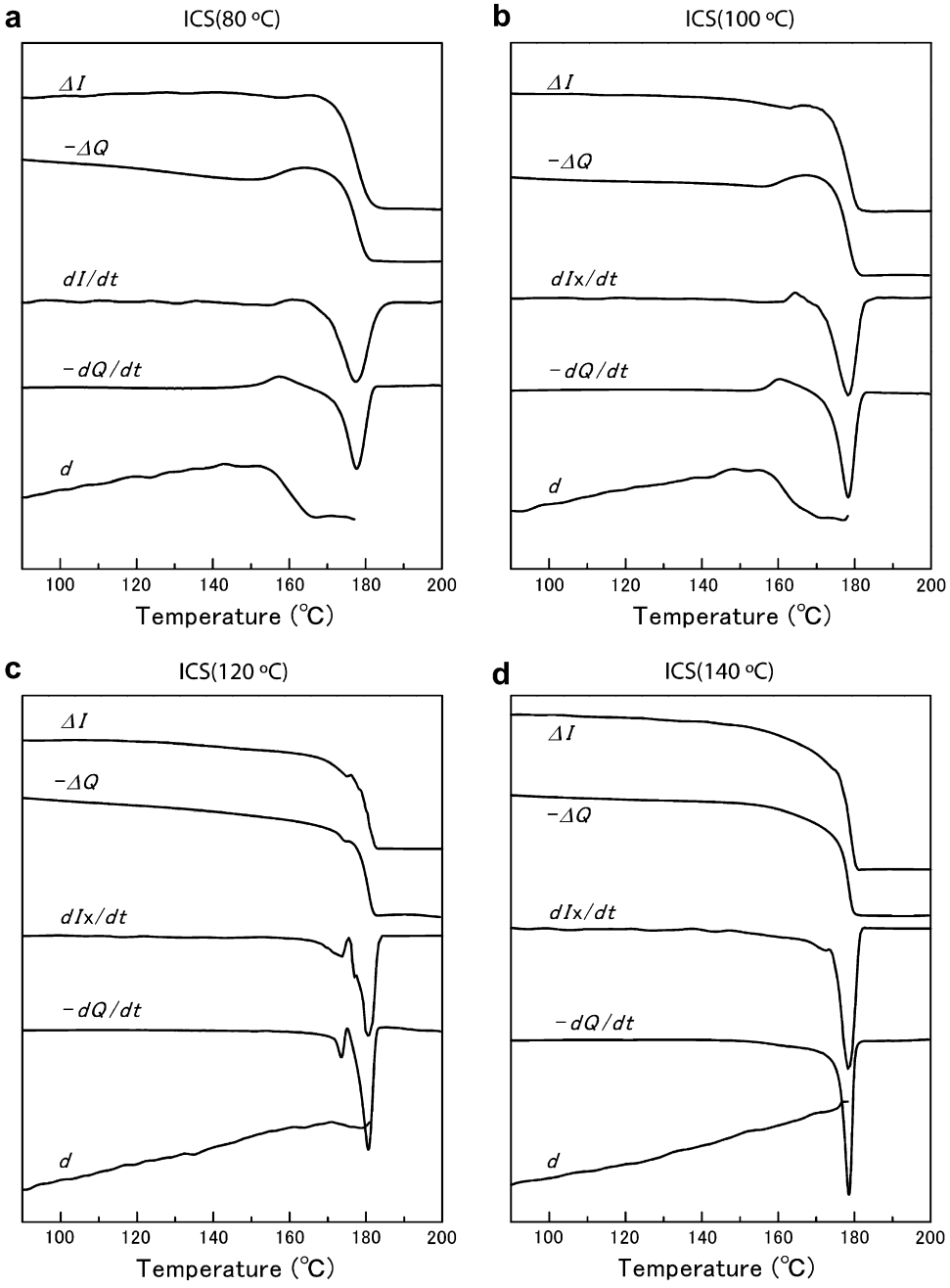

Fig. 8. Comparison of the data obtained with WAXD measurement and DSC: (a) ICS(80 °C), (b) ICS(100 °C), (c) ICS(120 °C), and (d) ICS(140 °C). Heating rate was 1.0 K min^{-1}.

The following points on the melting process of ICS(Region I) are suggested. The melt recrystallization and the phase transition from the α'-form to the α-form simultaneously occur in the transition region through the reorganization of chain molecules. The final melting peak, peak H in the DSC curve, corresponds to the melting of the α-form with high thermal stability formed through this process. The origin of these changes originates from the thermal expansion due to the thermal motion of the chain molecules in the frustrated crystal lattice.

Region II. With increasing temperature, as shown in Fig. 8, the lattice spacing (d) increases linearly up to 170 °C by the increase in the molecular motion, and then it is almost constant above this temperature. The melting and recrystallization competitively proceed in the heating process. The crystallinity (ΔI, $-\Delta Q$) decreases gradually up to 170 °C by the overwhelming of the melting by the increase in the molecular motion. Although the decreasing rate of the crystallinity increases above this temperature, the crystallinity abruptly increases by the recrystallization at about 175 °C. It may be deduced from these results that the large scale molecular motion in the molecular axis, which results in the recrystallization, occurs by the increase in the lattice spacing above this temperature.

Region III. As shown in Fig. 8, the lattice spacing (d) increases linearly up to the temperature of the final melting.

Although the melting and recrystallization competitively proceed in the heating process, the recrystallization does not overwhelm the melting. This result suggests that the large scale molecular motion in the molecular axis does not occur until the final melting in spite of the increase in the lattice spacing, because ordering of the crystalline lattice of the ICS-(Region III) is high. Accordingly, it is deduced that the melting and recrystallization proceed largely at above a certain lattice spacing which depends on the ordering of the crystalline lattice and degree of the perfection of the crystal.

4. Conclusions

Melting behavior of the ICS of PLLA was studied with X-ray and thermal analyses. Especially, this study was focused on the phase transition and the melt recrystallization during the melting process.

The transition of the crystal structure from the α'-form to the α-form of the ICSs(80, 100 °C) during the melting process was concluded from the appearance of the X-ray diffraction patterns of the α-form. The lattice spacing calculated from the main diffraction peak for the ICSs(80, 100 °C) increased with increasing temperature by thermal expansion. Then they obviously decreased in the temperature region around 155 °C and fitted to those of the ICSs(120, 140 °C) at about 165 °C. This result supports the phase transition from the α'-form to the α-form and suggests that there is a critical lattice spacing to start the transition from the α'-form to the α-form.

The diffraction patterns for the ICSs(120, 140 °C) did not change during the melting process, therefore X-ray analysis also gives conclusion that crystal structure of the α-form does not change during the melting process in Regions II and III. The X-ray result obviously denies a possibility of the interpretation of the two different crystal structures corresponding to the double endothermic peaks in the DSC curve in Region II.

The increase in the X-ray diffraction intensity before final melting in Regions I and II, which corresponds to an increase in crystallinity, gives a solid proof of the recrystallization during the melting process. Accordingly, the double melting behavior of PLLA can be concluded to originate from the increase in crystallinity through the melt recrystallization. The exothermic peak in the DSC curve can be conclusively attributed to the recrystallization. As shown in Fig. 8, $-\Delta Q$ and $\mathrm{d}I/\mathrm{d}T$ approximately coincided with ΔI and $-\mathrm{d}Q/\mathrm{d}t$, respectively, and a DSC curve could be reproduced by a temperature derivative curve of the diffraction intensity.

Acknowledgements

The authors would like to thank Professor Chitoshi Nakafuku (Kochi University, retired) for helpful suggestions and Dr. Shinsuke Tsubakihara (Fukuoka University) for X-ray analysis.

References

[1] Wunderlich B. Macromolecular physics, crystal melting, vol. III. New York: Academic Press; 1980.
[2] Celli A, Scandola M. Polymer 1992;33:2699.
[3] Nakafuku C, Sakoda M. Polym J 1993;25:909.
[4] Nakafuku C. Polym J 1994;26:680.
[5] Sarasua JR, Prud'homme RE, Wisniewski M, Borgne AL, Spassky N. Macromolecules 1998;31:3895.
[6] Fujita M, Doi Y. Biomacromolecules 2003;4:1301.
[7] Yasuniwa M, Tsubakihara S, Sugimoto Y, Nakafuku C. J Polym Sci Part B Polym Phys 2004;42:25.
[8] Sanchez MS, Ribelles JLG, Sanchez FH, Mano JF. Thermochim Acta 2005;430:201.
[9] Wang YM, Mano JF. Eur Polym J 2005;41:2335.
[10] Di Lorenzo ML. J Appl Polym Sci 2006;100:3145.
[11] Di Lorenzo ML. Macromol Symp 2006;234:176.
[12] Ling XY, Spruiell JE. J Polym Sci Part B Polym Phys 2006;44:3200.
[13] Ling XY, Spruiell JE. J Polym Sci Part B Polym Phys 2006;44:3378.
[14] Pan P, Kai W, Zhu B, Dong T, Inoue Y. Macromolecules 2006;40:6898.
[15] Shieh YT, Liu GL. J Polym Sci Part B Polym Phys 2007;45:466.
[16] Yasuniwa M, Iura K, Dan Y. Polymer 2007;48:5398.
[17] Zhang J, Duan Y, Sato H, Tsuji H, Noda I, Yan S, et al. Macromolecules 2005;38:8012.
[18] Yasuniwa M, Tsubakihara S, Ono Y, Dan Y, Takahashi K. Polymer 2006;47:7554.
[19] Zhang J, Tashiro K, Domb AJ, Tsuji H. Macromol Symp 2006;242:274.
[20] Cho T-Y, Strobl G. Polymer 2006;47:1036.
[21] Pan P, Zhu B, Kai W, Dong T, Inoue Y. J Appl Polym Sci 2008;107:54.
[22] Yasuniwa M, Tsubakihara S, Ohoshita K, Tokudome S. J Polym Sci Part B Polym Phys 2001;39:2005.
[23] Berry LG, editor. Powder diffraction file, inorganic volume, PD1S-10iRB. Philadelphia: Joint Committee on Powder Diffraction Standards; 1967. Sets 6–10 (revised).
[24] Yasuniwa M, Tsubakihara S, Satou T, Iura K. J Polym Sci Part B Polym Phys 2005;43:2039.
[25] Puiggali J, Ikada Y, Tsuji H, Lotz B. Polymer 2000;41:8921.
[26] Okihara T, Okumura K, Kawaguchi A. J Macromol Sci Phys 2003; B42:875.
[27] De Santis P, Kovacs A. Biopolymers 1968;6:299.
[28] Hoogsten W, Postema AR, Pennings AJ, Brinke G, Zugenmaier P. Macromolecules 1990;23:634.
[29] Kobayashi J, Asahi T, Ichiki M, Okikawa A, Suzuki H, Watanabe T, et al. J Appl Phys 1995;77:2957.
[30] Yasuniwa M, Tsubakihara S, Fujioka T. Thermochim Acta 2003; 396(1–2):75.
[31] Yasuniwa M, Tsubakihara S, Fujioka T, Dan Y. Polymer 2005;46:8306.